

Visualizing Kraus operators for dephasing noise during application of the $\sqrt{\text{SWAP}}$ quantum gate

Nicolas André da Costa Morazotti and Reginaldo de Jesus Napolitano
*São Carlos Institute of Physics, University of São Paulo,
PO Box 369, 13560-970, São Carlos, SP, Brazil*

We consider the case of a $\sqrt{\text{SWAP}}$ quantum gate and its optimized entangling action, via continuous dynamical decoupling, in the presence of dephasing noise. We illustrate the procedure in the specific case where only the two-qubit operation is controlled and no single-qubit operations are included in the description. To compare the optimized dynamics in the presence of noise with the ideal case, we use the standard fidelity measure. Then we discuss the importance of using optimized gates in the quantum operational-probabilistic theory. Because of their importance for the explicit construction of the completely positive maps representing the operations, we derive optimized Kraus operators in this specific case, focusing on the entanglement operation. We then show how to visualize the time evolution of each Kraus operator as a curve in a three-dimensional Euclidean space. Finally, we connect this formalism with the operational framework of quantum mechanics by describing a possible set of measurements that could be performed to obtain the Kraus operators.

I. INTRODUCTION

Optimal control has been a regularly studied subject for a long time, mainly for studies on spin dynamics [1], and it has become increasingly more relevant in the context of the quantum information science [2–4]. A very exciting prospect has been already envisaged starting in the first decade of the present century: the development of a quantum internet [5–7]. Recent experimental efforts have managed to establish a quantum-communication network over 4600 km [8]. In this context of quantum networking and communications, important topics have been referred to as transduction [9] and transfer of entanglement [10, 11]. In particular, flying qubits which get entangled on the fly with target qubits with which they interact have been considered in the context of scattering [12]. Inspired by these basic investigations, realistic implementation of distribution of entanglement over quantum networks is already occurring [13, 14]. However, all these possibilities are plagued by the unavoidable noise causing decoherence, which limits immensely the progress of implementation of quantum technologies, mainly when the carriers of quantum information are not photons [15]. It is, therefore, indispensable to understand the effects of quantum noise in quantum-information processing, including ways to correct for errors or to prevent them from happening [16].

Any quantum gate able to entangle two qubits together with general single-qubit operations will suffice for universal quantum processing [17]. Realization of entanglement between pairs of qubits by approaching and subsequently splitting them has been recently demonstrated using lattice surgery [18]. Also, addressability of individual qubits has even been extended to chromium molecules [19]. Indistinguishability symmetry has been explored in the context of entanglement and quantum control [20–22]. Along the lines of these particular recent developments, the $\sqrt{\text{SWAP}}$ gate has long been re-

alized in the laboratory using rubidium atoms in optical lattices, promising control over the effective exchange interaction [23]. Based on this possibility of articulating the time dependence of the effective interaction between two qubits, here we approach the case of quantum control of a $\sqrt{\text{SWAP}}$ entangling quantum gate in the presence of dephasing noise, which we simulate by introducing a boson bath. Relaxation times due to amplitude damping, because it involves transfer of energy by dissipation, are usually much longer than pure-decoherence times [24]. We, therefore, focus on the situation where we have the complete action of the $\sqrt{\text{SWAP}}$ gate fast compared to relaxation, but slow compared to dephasing.

We optimize the time dependence during the application of the entangling gate, while noise is present, by the well-studied continuous dynamical-decoupling procedure [25]. We compare the optimized noisy dynamics with the ideal, noiseless one by calculating the fidelity measure of our output operation. With the optimization of the gate under the perturbation due to coupling with the environment, we derive a set of corresponding Kraus operators [26, 27]. These operators provide the open-system evolution of any initial reduced matrix and are required to establish the completely positive maps representing the quantum operations in an Operational-Probabilistic Theory (OPT) of quantum mechanics [28–30]. Given the importance of the Kraus operators in the open-system dynamics of quantum-information processing, we present a prescription to visualize them via a one-to-one correspondence between each Kraus operator and a three-dimensional real vector. The whole dynamics as embedded in the time dependence of each Kraus operator is, thus, transcribed into the trajectory described by each of the corresponding vectors. Although our focus is on the $\sqrt{\text{SWAP}}$ gate under dephasing, we believe the visualization prescription may serve to inspire its generalization to more complex situations, analogously to the recent extension of the Bloch-sphere and Bloch-vector

concepts to the case of a qutrit [31] and, more generally, of a qudit [32].

In Sec. II we describe the optimization of the $\sqrt{\text{SWAP}}$ quantum gate in the presence of dephasing noise. In Sec. III we present our numerical calculations for the optimization of the time-dependence of the controlled entanglement, showing the fidelity measure as a function of several parameters involved in the simulations. In Sec. IV we calculate the optimized Kraus operators and present a prescription to their three-dimensional visualization. In Sec. V, in the spirit of Quantum Process Tomography (QPT) [33], we present a possible set of measurements illustrating how to obtain the process matrix [17] in the OPT language, which we briefly review in Appendix A. In Sec. VI we conclude our analysis and its results.

II. OPTIMIZATION OF THE $\sqrt{\text{SWAP}}$ QUANTUM GATE

The SWAP quantum gate has been considered both theoretically and experimentally [23] and, together with universal one-qubit operations, can be used to implement universal quantum computing [17]. Giving its importance, we investigate its optimal application by means of controlling its strength as a function of time to be optimized, as the experimental implementation of Ref. [23] has given evidence to its feasibility. Thus, we consider the gate Hamiltonian given by

$$H_G(t) = \hbar\Omega(t)G, \quad (1)$$

where G is an operator that acts on the two qubits, as we specify below, and $\Omega(t)$ is assumed to be a controlled frequency whose time dependence we can choose arbitrarily. Let us consider dephasing noise by introducing a boson field [24]. In this case, the total spin-boson Hamiltonian, much studied in the dissipative case [34, 35], can be written as

$$H(t) = H_G(t) + \hbar \sum_s \omega_s b_s^\dagger b_s + \hbar \sum_{k=1}^2 \sigma_{k,z} \sum_s (g_{k,s} b_s + g_{k,s}^* b_s^\dagger), \quad (2)$$

where ω_s is the frequency of the boson in its s th mode, b_s and b_s^\dagger are the annihilation and creation operators of a boson quantum in the s th mode, $\sigma_{k,z}$ is the z -axis Pauli matrix of the k th qubit, and $g_{k,s}$ is the coupling constant of the k th qubit with the s th boson degree of freedom. For concreteness, as we have emphasized above, let G describe the SWAP gate:

$$\begin{aligned} G &= |0\rangle\langle 0| \otimes |0\rangle\langle 0| + |1\rangle\langle 1| \otimes |1\rangle\langle 1| \\ &\quad + |0\rangle\langle 1| \otimes |1\rangle\langle 0| + |1\rangle\langle 0| \otimes |0\rangle\langle 1| \\ &= \frac{1}{2}\mathbb{I}_S + \frac{1}{2}\sigma_{1,x}\sigma_{2,x} + \frac{1}{2}\sigma_{1,y}\sigma_{2,y} + \frac{1}{2}\sigma_{1,z}\sigma_{2,z} \\ &= \frac{\mathbb{I}_S + \boldsymbol{\sigma}_1 \cdot \boldsymbol{\sigma}_2}{2}. \end{aligned} \quad (3)$$

Hence, it is easy to verify that

$$G^2 = \mathbb{I}_S, \quad (4)$$

where \mathbb{I}_S is the two-qubit identity operator. Here, the states of each qubit are given by the eigenstates of the Pauli operator for the z axis, forming the logical basis set: $\{|0\rangle, |1\rangle\}$. Conventionally, in the third line of Eq. (3) we adopt the indices $k = 1, 2$ as referring to the qubits whose operator factors in the tensor products are on the left and on the right, respectively.

In the absence of noise, that is, choosing $g_{k,s} = 0$ in Eq. (2), the simplest choice of $\Omega(t)$ that takes the factorized state $|0\rangle \otimes |1\rangle$, after a time interval τ , to a target state that is maximally entangled, namely,

$$|\psi(\tau)\rangle = \frac{1}{\sqrt{2}}|0\rangle \otimes |1\rangle - \frac{i}{\sqrt{2}}|1\rangle \otimes |0\rangle, \quad (5)$$

is simply a constant: $\Omega(t) = \pi/4\tau$.

Instead of the notation of Eq. (3) for the two-qubit kets and bras, henceforth we use a more compact notation for two-qubit logical kets in terms of their counterpart physical kets, namely, $|2m+n\rangle \equiv |m\rangle \otimes |n\rangle$ for $m, n \in \{0, 1\}$. The interaction between the qubits and the bosons in Eq. (2) does not couple the subspace spanned by $\{|0\rangle, |3\rangle\}$ to the one spanned by $\{|1\rangle, |2\rangle\}$. Furthermore, G only entangles the input states $|1\rangle$ and $|2\rangle$ in this new logical notation, that is, if we start with initial logical state $|0\rangle$ or $|3\rangle$, the dynamics driven by G , besides not leaving the subspace spanned by $\{|0\rangle, |3\rangle\}$, will not generate a superposition between $|0\rangle$ and $|3\rangle$. Therefore, since our purpose is to study optimized entangling evolutions, we just need to consider the logical subspace spanned by $\{|1\rangle, |2\rangle\}$ and, for concreteness, let us define the starting two-qubit state, at $t = 0$, as the one whose logical representation is given by the ket $|1\rangle$. We want to have an ideal superposition after gate G acts for a total time interval τ , which is the same as the one of Eq. (5), but that in the compact notation, in terms of the logical qubit, now reads:

$$|\psi(\tau)\rangle = \frac{1}{\sqrt{2}}|1\rangle - \frac{i}{\sqrt{2}}|2\rangle. \quad (6)$$

Restricted to the relevant subspace spanned by $\{|1\rangle, |2\rangle\}$, we have reduced the two-qubit physical system to a logical single-qubit system coupled with dephasing noise, so that now we can use, for G , the Pauli matrix σ_x acting on the logical basis as the exchange operator:

$$\sigma_x |1\rangle = |2\rangle \quad (7)$$

and

$$\sigma_x |2\rangle = |1\rangle. \quad (8)$$

In this simpler formulation, Eq. (2) is now mapped to the following total spin-boson Hamiltonian:

$$\begin{aligned} H_S(t) &= \hbar\Omega(t)\sigma_x + \hbar \sum_s \omega_s b_s^\dagger b_s \\ &\quad + \hbar\sigma_z \sum_s (g_s b_s + g_s^* b_s^\dagger), \end{aligned} \quad (9)$$

where

$$\sigma_z |1\rangle = |1\rangle, \quad (10)$$

$$\sigma_z |2\rangle = -|2\rangle, \quad (11)$$

and we have defined

$$g_s \equiv g_{1,s} - g_{2,s}. \quad (12)$$

To treat the effects of dephasing on the gate action, we now change to the interaction picture, that is, we transform from the global Schrödinger density-matrix operator $\rho(t)$ to its interaction-picture counterpart:

$$\rho_I(t) \equiv U_0^\dagger(t) \rho(t) U_0(t), \quad (13)$$

where

$$U_0(t) \equiv \exp[-i\Phi(t)\sigma_x] \exp\left(-i\sum_s \omega_s t b_s^\dagger b_s\right), \quad (14)$$

with

$$\Phi(t) \equiv \int_0^t dt' \Omega(t'). \quad (15)$$

It is now important to notice that $\rho(t)$ and $\rho_I(t)$ are meant to represent density-matrix operators of the whole system, that is, the system that is composed by the logical qubit and the thermal boson bath. Although we consider the initial qubit state as pure, given by

$$\rho_S(0) = |\psi(0)\rangle \langle\psi(0)|, \quad (16)$$

usually we take the initial state of the thermal bath, since it is thermal, as a mixed state, whose best description is in terms of its canonical density-matrix operator, namely,

$$\rho_B(0) = \frac{\exp(-\beta\hbar\sum_s \omega_s b_s^\dagger b_s)}{Z}, \quad (17)$$

where

$$\beta \equiv \frac{1}{k_B T}, \quad (18)$$

T is the boson-bath temperature, k_B is Boltzmann constant, and

$$Z \equiv \text{Tr}_B \left[\exp\left(-\beta\hbar\sum_s \omega_s b_s^\dagger b_s\right) \right] \quad (19)$$

is the partition function.

In the interaction picture, the corresponding evolution of the global density-matrix operator is given by

$$i\hbar \frac{d}{dt} \rho_I(t) = [H_I(t), \rho_I(t)], \quad (20)$$

with

$$\begin{aligned} H_I(t) &\equiv U_0^\dagger(t) H_{int} U_0(t) \\ &= \hbar\sigma_z(t) \sum_s [g_s b_s \exp(-i\omega_s t) \\ &\quad + g_s^* b_s^\dagger \exp(i\omega_s t)], \end{aligned} \quad (21)$$

where

$$\begin{aligned} \sigma_z(t) &\equiv [i\Phi(t)\sigma_x] \sigma_z \exp[-i\Phi(t)\sigma_x] \\ &= \sigma_z \cos[2\Phi(t)] + \sigma_y \sin[2\Phi(t)]. \end{aligned} \quad (22)$$

The interaction-picture global dynamics are thus dictated by Eq. (20) and are, therefore, unitary. That is to say that there is a unitary operator, $U_I(t)$, acting on the qubit and the boson bath, such that

$$\rho_I(t) = U_I(t) \rho_I(0) U_I^\dagger(t), \quad (23)$$

with

$$i\hbar \frac{d}{dt} U_I(t) = H_I(t) U_I(t) \quad (24)$$

and

$$U_I(0) = \mathbb{I}_S \otimes \mathbb{I}_B, \quad (25)$$

where \mathbb{I}_B is the unitary operator acting on the boson Hilbert space. In Eq. (23), the initial global state here is prepared at $t=0$ as a factored state:

$$\rho_I(0) = \rho_S(0) \rho_B(0), \quad (26)$$

where $\rho_S(0)$ and $\rho_B(0)$ are given by Eqs. (16) and (17), respectively. From Eqs. (23) and (26), it follows that

$$\rho_{IS}(t) = \text{Tr}_B \left[U_I(t) \rho_S(0) \rho_B(0) U_I^\dagger(t) \right], \quad (27)$$

which is the reduced density operator that describes the state of the logical qubit, also in the interaction picture.

From now on let us adopt the convenient index notation in which $(\mathbb{I}_S, \sigma_x, \sigma_y, \sigma_z) = (\sigma_0, \sigma_1, \sigma_2, \sigma_3)$. We thus can write

$$U_I(t) = \sum_{\mu=0}^3 B_\mu(t) \sigma_\mu, \quad (28)$$

noticing that the operators $B_\mu(t)$, for $\mu=0,1,2,3$, act only on the boson states. Using Eqs. (27) and (28), we obtain

$$\rho_{IS}(t) = \sum_{\mu=0}^3 \sum_{\nu=0}^3 \sigma_\mu \rho_S(0) \sigma_\nu M_{\nu,\mu}(t), \quad (29)$$

where we have defined the process-matrix elements [17]:

$$M_{\nu,\mu}(t) \equiv \text{Tr}_B [B_\nu^\dagger(t) B_\mu(t) \rho_B(0)]. \quad (30)$$

All we have to do next is to calculate the functions $M_{\nu,\mu}(t)$, for $\nu, \mu \in \{0,1,2,3\}$.

III. NUMERICAL SIMULATIONS

Our simulations can be carried out by solving the master equation [36, 37],

$$\frac{d}{dt}\rho_{IS}(t) = -\frac{1}{\hbar^2}\text{Tr}_B \left\{ \int_0^t dt' [H_I(t), [H_I(t'), \rho_B(0)\rho_{IS}(t)]] \right\}, \quad (31)$$

or by solving directly the Bloch-vector trajectory equation [25],

$$\frac{d}{dt}\mathbf{r}(t) = -4\mathbf{\Lambda}(t) \times \text{Im}[\mathbf{G}(t)] - 4\mathbf{\Lambda}(t) \times \{\mathbf{r}(t) \times \text{Re}[2\mathbf{F}(t) + \mathbf{G}(t)]\}. \quad (32)$$

It is relevant to emphasize that Eq. (31) is time local and it applies to non-Markovian situations, including the present case, where we assume that the control by continuous dynamical decoupling is faster than the correlation time of the bath operators [25]. Equation (32) is derived from Eq. (31) using the convenient definitions:

$$\mathbf{\Lambda}(t) \equiv \hat{\mathbf{z}} \cos[2\Phi(t)] + \hat{\mathbf{y}} \sin[2\Phi(t)], \quad (33)$$

$$\mathbf{F}(t) \equiv \int_0^t dt' \mathbf{\Lambda}(t') \mathcal{I}_1(t-t'), \quad (34)$$

$$\mathbf{G}(t) \equiv \int_0^t dt' \mathbf{\Lambda}(t') \mathcal{I}_2(t-t'), \quad (35)$$

$$\mathcal{I}_1(t) \equiv \sum_s |g_s|^2 \frac{\exp(i\omega_s t)}{\exp(\beta\hbar\omega_s) - 1}, \quad (36)$$

and

$$\mathcal{I}_2(t) \equiv \sum_s |g_s|^2 \exp(i\omega_s t). \quad (37)$$

The Bloch vector, $\mathbf{r}(t)$, is related with the reduced density-matrix operator in the interaction picture, $\rho_{IS}(t)$, as [38]

$$\rho_{IS}(t) = \frac{1}{2}\mathbb{I}_S + \frac{1}{2}\mathbf{r}(t) \cdot \boldsymbol{\sigma}. \quad (38)$$

If we write

$$\mathbf{r}(t) = \hat{\mathbf{x}}x_1(t) + \hat{\mathbf{y}}x_2(t) + \hat{\mathbf{z}}x_3(t), \quad (39)$$

we can calculate the Bloch vector from the density operator by

$$\mathbf{r}(t) = \text{Tr}[\boldsymbol{\sigma}\rho_{IS}(t)], \quad (40)$$

where the trace without a subscript stands for the trace of 2×2 matrices. Of course, the initial condition for the Bloch vector is easily calculated using Eq. (40) at $t = 0$ and Eq. (16).

For the sake of our emulation of dephasing we simplify the structure of the noise by assuming an Ohmic spectral density [39], namely,

$$J(\omega) \equiv \sum_s |g_s|^2 \delta(\omega - \omega_s), \quad (41)$$

with

$$J(\omega) = \eta\omega \exp\left(-\frac{\omega}{\omega_c}\right). \quad (42)$$

Here, ω_c is a cutoff frequency and η is a dimensionless noise strength. Using Eqs. (41) and (42) in Eqs. (36) and (37), we obtain:

$$\mathcal{I}_1(t) = \frac{\eta}{\beta^2\hbar^2}\psi^{(1)}\left(1 + \frac{1}{\beta\omega_c\hbar} - \frac{it}{\beta\hbar}\right), \quad (43)$$

where $\psi^{(1)}(z)$ is the first polygamma function [40], and

$$\mathcal{I}_2(t) = \frac{\eta\omega_c^2}{(1 - i\omega_c t)^2}. \quad (44)$$

To set up our numerical investigations, we establish the numerical values to characterize the effects of the phase noise. Let us, thus, look only at the decoherence that the noise produces by choosing $\Omega(t) = 0$ in Eq. (1) and starting with an initially pure density matrix $\rho_S(0) = |\psi_0\rangle\langle\psi_0|$ derived from the initial qubit state

$$|\psi_0\rangle \equiv c_1|1\rangle + c_2|2\rangle, \quad (45)$$

where c_1 and c_2 are two complex constants such that

$$|c_1|^2 + |c_2|^2 = 1. \quad (46)$$

Since there is no quantum gate action and Eq. (45) is an arbitrary coherent state, what we describe here are the effects of the dephasing noise in a quantum memory, where the bath perturbation destroys the coherence and, hence, the quantum information stored in the qubit system. As is derived in Appendix B, the exact analytical solution of the Schrödinger equation using the interaction-picture Hamiltonian of Eq. (21), for the spectral density of Eqs. (41) and (42) and the initial state of Eq. (45), in the absence of a quantum gate, that is, for $\Omega(t) = 0$, produces a reduced density matrix in the interaction picture given by:

$$\rho_{IS}^{\text{pure noise}}(t) = \begin{pmatrix} |c_1|^2 & c_1c_2^*\xi(t) \\ c_1^*c_2\xi(t) & |c_2|^2 \end{pmatrix}, \quad (47)$$

where

$$\xi(t) \equiv \left\{ \frac{\left| \left(\frac{k_B T}{\hbar\omega_c} + i\frac{k_B T}{\hbar}t \right)! \right|^4}{\left(1 + \omega_c^2 t^2 \right) \left[\left(\frac{k_B T}{\hbar\omega_c} \right)! \right]^4} \right\}^{2\eta}. \quad (48)$$

Here, of course, we are using the factorial notation for the gamma function [40]:

$$\begin{aligned} z! &\equiv \Gamma(z+1) \\ &= \int_0^\infty ds \exp(-s) s^z, \end{aligned} \quad (49)$$

for $\text{Re}(z) > -1$. In the interaction picture, the fidelity measure, at an instant t , when we have an ideal pure state $\rho_{IS}^{\text{ideal}}(t) = \rho_S(0)$ and a general state $\rho_{IS}(t)$, is given by [41, 42]:

$$F(t) \equiv \text{Tr}[\rho_{IS}(t) \rho_S(0)]. \quad (50)$$

Figure 1 shows

$$F_0(t) \equiv \langle \psi_0 | \rho_{IS}^{\text{pure noise}}(t) | \psi_0 \rangle, \quad (51)$$

which results from Eq. (50) for the case of pure noise, where we use $\Omega(t) = 0$, $\eta = 0.01$, $\omega_c = 8\pi/\tau$, $T = \hbar\omega_c/k_B$, and $c_1 = ic_2 = 1/\sqrt{2}$ in Eq. (45). The final value of the fidelity, in this case, is

$$F_0(\tau) \approx 0.5296. \quad (52)$$

It is important to notice that this exact result agrees perfectly well with our numerical calculations using the master equation of Eqs. (31) and (32).

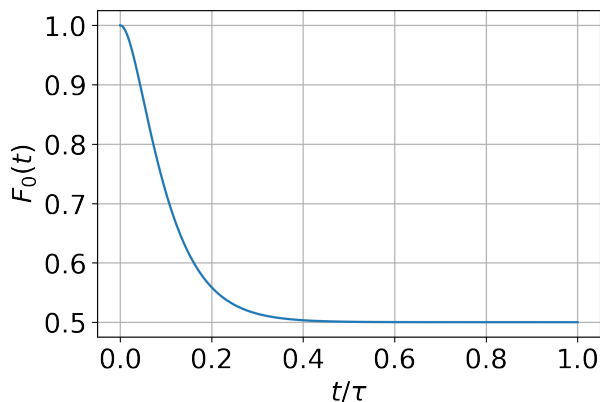


Figure 1: The fidelity of Eq. (51) as a function of time for pure noise. We use $\Omega(t) = 0$, $\eta = 0.01$, $\omega_c = 8\pi/\tau$, $T = \hbar\omega_c/k_B$, and $c_1 = ic_2 = 1/\sqrt{2}$ in Eq. (45). The final value of the fidelity, in this case, is $F_0(\tau) \approx 0.5296$.

Now that we have compared our numerical simulations against the exact analytical result, we turn back to the case with $\Omega(t) \neq 0$, for which we do not have an analytic result and, thus, we use Eqs. (31) and (32) to calculate numerically the reduced density matrix as a function of time. As mentioned at the beginning of Sec. II, we take $|1\rangle$ as the initial state, that is, $\rho_S(0) = |1\rangle\langle 1|$ and calculate the final fidelity using Eq. (50) with $\Omega(t) = \pi/4\tau$, $\omega_c = 8\pi/\tau$, $T = \hbar\omega_c/k_B$, and two values of the noise strength: $\eta = 0.01$ and $\eta = 0.05$. The fidelities we obtain at $t = \tau$ for each of these values of η are, respectively,

$$F_{\eta=0.01}(\tau) \approx 0.691 \quad (53)$$

and

$$F_{\eta=0.05}(\tau) \approx 0.586. \quad (54)$$

Figure 2 shows the fidelities $F_{\eta=0.01}(t)$ and $F_{\eta=0.05}(t)$ as functions of time.

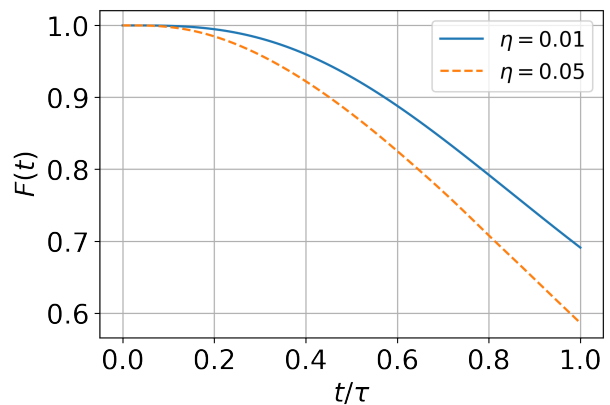


Figure 2: The fidelity of Eq. (50) as a function of time when we have $\rho_S(0) = |1\rangle\langle 1|$, $\Omega(t) = \pi/4\tau$, $\omega_c = 8\pi/\tau$, $T = \hbar\omega_c/k_B$, and two values of the noise strength: $\eta = 0.01$ and $\eta = 0.05$. The fidelities we obtain at $t = \tau$ for each of these values of η are, respectively, $F_{\eta=0.01}(\tau) \approx 0.691$ and $F_{\eta=0.05}(\tau) \approx 0.586$.

We are now able to calculate the trajectories described by the Bloch-vector evolution calculated using Eq. (32). Figure 3 shows, as illustrations, the trajectories for the cases whose final fidelities are given by Eqs. (53) and (54).

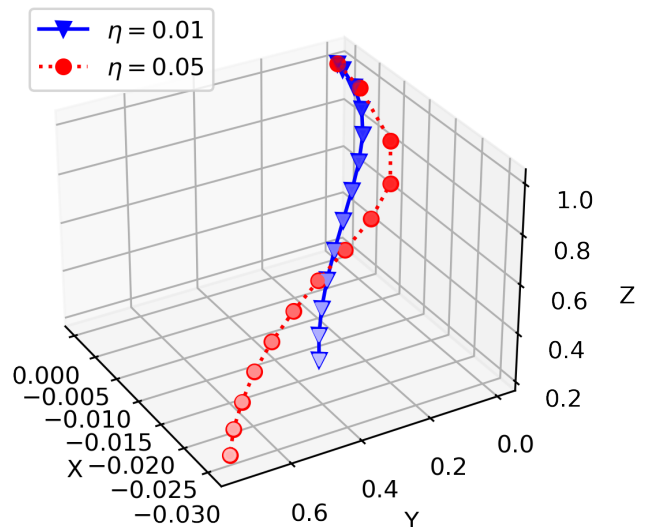


Figure 3: Bloch-vector trajectories obtained by solving Eq. (32) when we have $\rho_S(0) = |1\rangle\langle 1|$, $\Omega(t) = \pi/4\tau$, $\omega_c = 8\pi/\tau$, and $T = \hbar\omega_c/k_B$, for $\eta = 0.01$ and $\eta = 0.05$, in which cases we obtain the final fidelities of Eqs. (53) and (54), that is, $F_{\eta=0.01}(\tau) \approx 0.691$ and $F_{\eta=0.05}(\tau) \approx 0.586$, respectively. Time evolution proceeds from darker to lighter. For $\eta = 0.01$, $\mathbf{r}(\tau) = -0.028\hat{x} + 0.45\hat{y} + 0.38\hat{z}$. For $\eta = 0.05$, $\mathbf{r}(\tau) = -0.03\hat{x} + 0.74\hat{y} + 0.17\hat{z}$.

The optimization procedure we adopt here is called the continuous dynamical decoupling of phase noise, as pre-

scribed in Ref. [25]. Accordingly, for protecting against dephasing, in the case of our Hamiltonian of Eq. (9), we simply have to choose a constant $\Omega(t)$ given by

$$\Omega(t) = \frac{\pi}{4\tau} + \frac{2n\pi}{\tau}, \quad (55)$$

with $n \in \mathbb{Z}$. The final fidelity at $t = \tau$ will approach unity as the magnitude of n is sufficiently increased. Figure 4 shows the fidelity measures as functions of time, Eq. (50), using different values of n appearing in Eq. (55). In the simulations of Fig. 4 we have used $\rho_S(0) = |1\rangle\langle 1|$, $\omega_c = 8\pi/\tau$, $T = \hbar\omega_c/k_B$, $\eta = 0.05$, and $\Omega(t)$ as given by Eq. (55), for the cases where $n = 0$, $n = 6$, $n = 12$, $n = 15$, and $n = 30$. Table I shows the final fidelity measures, Eq. (50), for these choices of n .

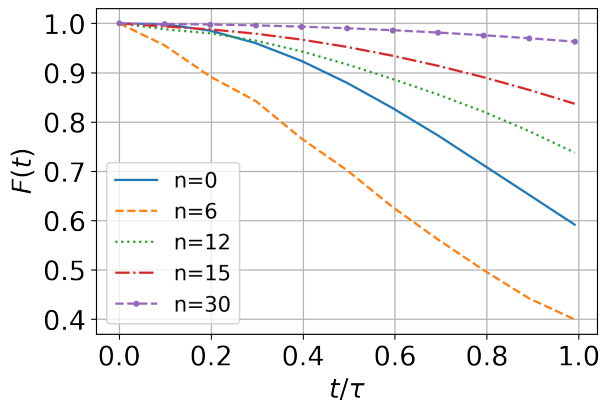


Figure 4: Fidelity measures as functions of time, Eq. (50), using different values of n appearing in Eq. (55).

Here we have used $\rho_S(0) = |1\rangle\langle 1|$, $\omega_c = 8\pi/\tau$, $T = \hbar\omega_c/k_B$, $\eta = 0.05$, and $\Omega(t)$ as given by Eq. (55), for the cases where $n = 0$, $n = 6$, $n = 12$, $n = 15$, and $n = 30$.

n in Eq. (55)	0	6	12	15	30
$F(\tau)$ from Eq. (50)	0.586	0.391	0.734	0.836	0.962
$ \mathbf{r}(\tau) - \mathbf{r}(0) $	1.11	1.46	0.97	0.78	0.38

Table I: Final fidelities at $t = \tau$, Eq. (50), with $\rho_S(0) = |1\rangle\langle 1|$, $\omega_c = 8\pi/\tau$, $T = \hbar\omega_c/k_B$, $\eta = 0.05$, and $\Omega(t)$ as given by Eq. (55), for $n = 0$, $n = 6$, $n = 12$, $n = 15$, and $n = 30$. Also shown is the distance between the final Bloch vector, $\mathbf{r}(\tau)$, and its initial value, $\mathbf{r}(0) = \hat{\mathbf{z}}$, as a function of n for the values chosen.

It is interesting that as n increases the final fidelity initially decreases and, after n reaches a sufficiently higher magnitude the fidelity starts to approach unity monotonically. Specifically for the choice of parameters and initial state of Fig. 4, we observe that the final fidelity progressively decreases to values lower than the one for $n = 0$, Eq. (54), as n is changed from $n = 1$ to $n = 5$,

and then increases monotonically with $n \geq 6$, surpassing the value given by Eq. (54) for $n \geq 10$.

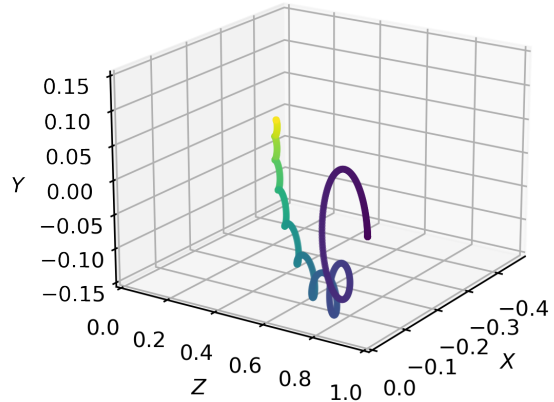


Figure 5: The Bloch-vector trajectory when $n = 2$ for $\rho_S(0) = |1\rangle\langle 1|$, $\omega_c = 8\pi/\tau$, $T = \hbar\omega_c/k_B$, $\eta = 0.05$, and $\Omega(t)$ as given by Eq. (55). Time evolution proceeds from purple (darker) to yellow (lighter). It starts at $\mathbf{r}(0) = \hat{\mathbf{z}}$ and ends at $\mathbf{r}(\tau) = -0.485\hat{\mathbf{x}} - 0.024\hat{\mathbf{y}} - 0.045\hat{\mathbf{z}}$.

As an illustration of a trajectory traced by the evolution of a Bloch vector under continuous dynamical decoupling, Fig. 5 shows such a curve corresponding to the case with $n = 2$ when $\rho_S(0) = |1\rangle\langle 1|$, $\omega_c = 8\pi/\tau$, $T = \hbar\omega_c/k_B$, $\eta = 0.05$, and $\Omega(t)$ as given by Eq. (55). In the interaction picture, if n is large enough, the distance between $\mathbf{r}(\tau)$ and $\mathbf{r}(0)$ gradually decreases, as is also shown in Table I. Moreover, as n increases, the frequency $\Omega(t)$, Eq. (55), gets large and the helical aspect of the Bloch-vector trajectories becomes progressively more pronounced than the one shown in Fig. 5 for $n = 2$.

Once we obtain the Bloch-vector trajectory, $\mathbf{r}(t)$, or, equivalently, the density matrix, $\rho_{IS}(t)$, as functions of time, we must calculate the functions given by Eq. (30). We have proceeded as follows. From Eq. (29) we see that the matrix elements $M_{\nu,\mu}(t)$ do not depend on the initial condition. Therefore, we can choose different initial conditions to obtain a sufficient number of equations that we can then solve to obtain all these elements. Accordingly, we have chosen the following four different initial conditions for the components of the Bloch vector:

$$x_{k,\mu}(0) = \delta_{k,\mu}, \quad (56)$$

for $k = 1, 2, 3$ and $\mu = 0, 1, 2, 3$. Now, after time $t > 0$, we will have four evolved Bloch vectors given by

$$\mathbf{r}_\mu(t) \equiv \hat{\mathbf{x}}x_{1,\mu}(t) + \hat{\mathbf{y}}x_{2,\mu}(t) + \hat{\mathbf{z}}x_{3,\mu}(t), \quad (57)$$

for $\mu = 0, 1, 2, 3$. Using the initial conditions of Eq. (56), we obtain the following equations to solve for the process-matrix elements $M_{\nu,\mu}(t)$:

$$\sum_{\alpha=0}^3 \sum_{\beta=0}^3 \sigma_{\alpha} \left[\frac{1}{2} \mathbb{I}_S + \frac{1}{2} \mathbf{r}_{\mu}(0) \cdot \boldsymbol{\sigma} \right] \sigma_{\beta} M_{\beta, \alpha}(t) = \frac{1}{2} \mathbb{I}_S + \frac{1}{2} \mathbf{r}_{\mu}(t) \cdot \boldsymbol{\sigma}, \quad (58)$$

for $\mu = 0, 1, 2, 3$, where we have used Eqs. (29) and (38), together with the initial conditions given by Eq. (56). Here, of course, $\mathbf{r}_{\mu}(t)$ are the evolved Bloch vectors obtained using the corresponding initial conditions given by Eq. (57). By solving Eq. (58) explicitly, we obtain:

$$M_{0,0} = \frac{1}{4} (-x_{1,0} + x_{1,1} - x_{2,0} + x_{2,2} - x_{3,0} + x_{3,3} + 1), \quad (59)$$

$$M_{0,1} = \frac{1}{4} (x_{1,0} - ix_{2,0} + ix_{2,3} + ix_{3,0} - ix_{3,2}), \quad (60)$$

$$M_{0,2} = \frac{1}{4} i (x_{1,0} - x_{1,3} - ix_{2,0} - x_{3,0} + x_{3,1}), \quad (61)$$

$$M_{0,3} = -\frac{1}{4} i (x_{1,0} - x_{1,2} - x_{2,0} + x_{2,1} + ix_{3,0}), \quad (62)$$

$$M_{1,0} = \frac{1}{4} (x_{1,0} + ix_{2,0} - ix_{2,3} - ix_{3,0} + ix_{3,2}), \quad (63)$$

$$M_{1,1} = \frac{1}{4} (-x_{1,0} + x_{1,1} + x_{2,0} - x_{2,2} + x_{3,0} - x_{3,3} + 1), \quad (64)$$

$$M_{1,2} = \frac{1}{4} (-x_{1,0} + x_{1,2} - x_{2,0} + x_{2,1} + ix_{3,0}), \quad (65)$$

$$M_{1,3} = \frac{1}{4} (-x_{1,0} + x_{1,3} - ix_{2,0} - x_{3,0} + x_{3,1}), \quad (66)$$

$$M_{2,0} = -\frac{1}{4} i (x_{1,0} - x_{1,3} + ix_{2,0} - x_{3,0} + x_{3,1}), \quad (67)$$

$$M_{2,1} = \frac{1}{4} (-x_{1,0} + x_{1,2} - x_{2,0} + x_{2,1} - ix_{3,0}), \quad (68)$$

$$M_{2,2} = \frac{1}{4} (x_{1,0} - x_{1,1} - x_{2,0} + x_{2,2} + x_{3,0} - x_{3,3} + 1), \quad (69)$$

$$M_{2,3} = \frac{1}{4} i (x_{1,0} + ix_{2,0} - ix_{2,3} + ix_{3,0} - ix_{3,2}), \quad (70)$$

$$M_{3,0} = \frac{1}{4} i (x_{1,0} - x_{1,2} - x_{2,0} + x_{2,1} - ix_{3,0}), \quad (71)$$

$$M_{3,1} = \frac{1}{4} (-x_{1,0} + x_{1,3} + ix_{2,0} - x_{3,0} + x_{3,1}), \quad (72)$$

$$M_{3,2} = -\frac{1}{4} i (x_{1,0} - ix_{2,0} + ix_{2,3} - ix_{3,0} + ix_{3,2}), \quad (73)$$

$$M_{3,3} = \frac{1}{4} (x_{1,0} - x_{1,1} + x_{2,0} - x_{2,2} - x_{3,0} + x_{3,3} + 1), \quad (74)$$

where, we have simplified the notation by writing $M_{\nu, \mu} = M_{\nu, \mu}(t)$ and $x_{k, \mu} = x_{k, \mu}(t)$, with $k \in \{1, 2, 3\}$ and $\nu, \mu \in \{0, 1, 2, 3\}$.

IV. VISUALIZATION OF KRAUS OPERATORS

As can be seen from Eq. (30), the matrix whose elements are the functions $M_{\nu, \mu}(t)$ is Hermitian. Therefore, it can be diagonalized as

$$\sum_{\gamma=0}^3 W_{\gamma, \mu}^*(t) D_{\gamma}(t) W_{\gamma, \nu}(t) = M_{\mu, \nu}(t), \quad (75)$$

where the matrix whose elements are $W_{\gamma, \nu}(t)$ is unitary and $D_{\gamma}(t)$, for $\gamma = 0, 1, 2, 3$, can be easily shown to be non-negative real numbers. The Kraus operators [26, 27] are, therefore, defined as [17]

$$K_{\gamma}(t) \equiv \exp[i\chi_{\gamma}(t)] \sum_{\mu=0}^3 \sqrt{D_{\gamma}(t)} W_{\gamma, \mu}(t) \sigma_{\mu} \quad (76)$$

and

$$K_{\gamma}^{\dagger}(t) \equiv \exp[-i\chi_{\gamma}(t)] \sum_{\mu=0}^3 \sqrt{D_{\gamma}(t)} W_{\gamma, \mu}^*(t) \sigma_{\mu}, \quad (77)$$

where $\chi_{\gamma}(t)$, for $\gamma = 0, 1, 2, 3$, are arbitrary real functions, since each Kraus operator can be defined up to a global phase factor. We are going to make good use of this freedom in what follows. Next we show, for the present case of the $\sqrt{\text{SWAP}}$ gate under dephasing, how to visualize the evolution of $K_{\gamma}(t)$.

Equations (21), (22), (24), and (28) imply the following coupled matrix equations giving the dynamics of the boson field operators $B_{\mu}(t)$, for $\mu = 0, 1, 2, 3$:

$$i\hbar \frac{d}{dt} \begin{bmatrix} B_0(t) \\ B_1(t) \end{bmatrix} = \begin{bmatrix} \sin[2\Phi(t)] & \cos[2\Phi(t)] \\ -i \cos[2\Phi(t)] & i \sin[2\Phi(t)] \end{bmatrix} H_{BI}(t) \begin{bmatrix} B_2(t) \\ B_3(t) \end{bmatrix} \quad (78)$$

and

$$i\hbar \frac{d}{dt} \begin{bmatrix} B_2(t) \\ B_3(t) \end{bmatrix} = \begin{bmatrix} \sin[2\Phi(t)] & i \cos[2\Phi(t)] \\ \cos[2\Phi(t)] & -i \sin[2\Phi(t)] \end{bmatrix} H_{BI}(t) \begin{bmatrix} B_0(t) \\ B_1(t) \end{bmatrix}, \quad (79)$$

where we have defined the boson Hamiltonian $H_{BI}(t)$ in the interaction picture as

$$H_{BI}(t) \equiv \hbar \sum_s [g_s b_s \exp(-i\omega_s t) + g_s^* b_s^\dagger \exp(i\omega_s t)]. \quad (80)$$

Given the initial condition for $U_I(t)$, Eq. (25), we obtain, according with Eq. (28), the initial conditions for the field operators, namely,

$$\begin{bmatrix} B_0(0) \\ B_1(0) \\ B_2(0) \\ B_3(0) \end{bmatrix} = \begin{bmatrix} 1 \\ 0 \\ 0 \\ 0 \end{bmatrix}. \quad (81)$$

Hence, formal integration of Eq. (79) from $t = 0$ to t' and, after using Eq. (81), substituting the resulting expression into Eq. (78), gives

$$i\hbar \frac{d}{dt} \begin{bmatrix} B_0(t) \\ B_1(t) \end{bmatrix} = \frac{1}{i\hbar} \int_0^t dt' \begin{bmatrix} \cos[\zeta(t, t')] & i \sin[\zeta(t, t')] \\ i \sin[\zeta(t, t')] & \cos[\zeta(t, t')] \end{bmatrix} \times H_{BI}(t) H_{BI}(t') \begin{bmatrix} B_0(t') \\ B_1(t') \end{bmatrix}, \quad (82)$$

where

$$\zeta(t, t') \equiv 2\Phi(t) - 2\Phi(t'). \quad (83)$$

Equation (82) is easily diagonalized by the time-independent Hermitian and unitary matrix

$$S \equiv \frac{1}{\sqrt{2}} \begin{bmatrix} 1 & 1 \\ 1 & -1 \end{bmatrix}. \quad (84)$$

By defining the c -number function

$$h(t) \equiv - \sum_s |g_s|^2 2i \int_0^t dt' \int_0^{t'} dt'' \exp[-i\zeta(t', t'')] \times \sin[\omega_s(t'' - t')], \quad (85)$$

we can express the solution of Eq. (82) as

$$\begin{bmatrix} B_0(t) \\ B_1(t) \end{bmatrix} = \frac{1}{2} \begin{bmatrix} \Gamma(t) + \exp[h(t)] [\Gamma(t)]^\dagger \\ \Gamma(t) - \exp[h(t)] [\Gamma(t)]^\dagger \end{bmatrix}, \quad (86)$$

where the operator boson field $\Gamma(t)$ satisfies the integro-differential equation:

$$\frac{d}{dt} \Gamma(t) = -\frac{1}{\hbar^2} \int_0^t dt' \exp[i\zeta(t, t')] \times H_{BI}(t) H_{BI}(t') \Gamma(t'), \quad (87)$$

with

$$\Gamma(0) = \mathbb{I}_B. \quad (88)$$

Equation (87) is solved iteratively, as in the usual time-dependent perturbation theory.

Next we observe that Eq. (87) shows that $\Gamma(t)$ results in an operator consisting of a series, each term of which contains an even number of creation (b_s^\dagger) and/or annihilation operators (b_s) as factors. This means that, according with Eq. (86), the operators $B_0(t)$ and $B_1(t)$ will also be series of terms containing only an even number of boson-operator factors. However, as we see from Eq. (79), because of the extra Hamiltonian factor, $B_2(t)$ and $B_3(t)$ will be operator series whose terms each contains an odd number of boson-operator factors. Therefore, it follows from Eqs. (17) and (30) that

$$M_{0,2}(t) = M_{2,0}(t) = 0, \quad (89)$$

$$M_{0,3}(t) = M_{3,0}(t) = 0, \quad (90)$$

$$M_{1,2}(t) = M_{2,1}(t) = 0, \quad (91)$$

and

$$M_{1,3}(t) = M_{3,1}(t) = 0. \quad (92)$$

We can, thus, arrange the elements $M_{\nu,\mu}(t)$, for $\nu, \mu \in \{0, 1, 2, 3\}$, as a block-diagonal process matrix [17]:

$$M(t) = \begin{bmatrix} M_{0,0}(t) & M_{0,1}(t) & 0 & 0 \\ M_{0,1}^*(t) & M_{1,1}(t) & 0 & 0 \\ 0 & 0 & M_{2,2}(t) & M_{2,3}(t) \\ 0 & 0 & M_{2,3}^*(t) & M_{3,3}(t) \end{bmatrix}. \quad (93)$$

Diagonalization of Eq. (93) is analytical in terms of the elements $M_{\nu,\mu}(t)$, for $\nu, \mu \in \{0, 1, 2, 3\}$. Each of the two 2×2 blocks, for each instant t , is of the form

$$A = \begin{bmatrix} c & a + bi \\ a - bi & d \end{bmatrix}, \quad (94)$$

where $a, b, c, d \in \mathbb{R}$. To simplify the notation, let us write

$$a + bi \equiv \sqrt{a^2 + b^2} \exp(i\varphi) \equiv \rho \exp(i\varphi) \quad (95)$$

and

$$\delta \equiv \frac{c - d}{2}. \quad (96)$$

We can, thus, by the usual textbook methods, obtain the diagonalizing matrix $W(t)$, whose elements are $W_{\gamma,\nu}(t)$, for $\gamma, \nu \in \{0, 1, 2, 3\}$, appearing in Eq. (75):

$$W(t) = \begin{bmatrix} u_+^* & u_-^* & 0 & 0 \\ u_- & -u_+ & 0 & 0 \\ 0 & 0 & \tilde{u}_+^* & \tilde{u}_-^* \\ 0 & 0 & \tilde{u}_- & -\tilde{u}_+ \end{bmatrix}, \quad (97)$$

where

$$\begin{bmatrix} u_+ \\ u_- \end{bmatrix} = \frac{1}{\sqrt{2}} \begin{bmatrix} \exp(i\frac{\varphi}{2}) \sqrt{1 + \frac{\delta}{\sqrt{\delta^2 + \rho^2}}} \\ \exp(-i\frac{\varphi}{2}) \sqrt{1 - \frac{\delta}{\sqrt{\delta^2 + \rho^2}}} \end{bmatrix} \quad (98)$$

and a completely analogous expression for the block involving \tilde{u}_+ and \tilde{u}_- . Of course, since Eq. (94) is only a simplified notation for each time-dependent block of Eq. (93), all the non-zero elements of $W(t)$ are also functions of t .

After diagonalizing $M(t)$, we obtain the elements $D_\gamma(t)$, for $\gamma = 0, 1, 2, 3$, appearing in Eq. (75):

$$D_0(t) \equiv \frac{c+d}{2} + \sqrt{\delta^2 + \rho^2}, \quad (99)$$

$$D_1(t) \equiv \frac{c+d}{2} - \sqrt{\delta^2 + \rho^2}, \quad (100)$$

$$D_2(t) \equiv \frac{\tilde{c} + \tilde{d}}{2} + \sqrt{\tilde{\delta}^2 + \tilde{\rho}^2}, \quad (101)$$

and

$$D_3(t) \equiv \frac{\tilde{c} + \tilde{d}}{2} - \sqrt{\tilde{\delta}^2 + \tilde{\rho}^2}, \quad (102)$$

where, as above, we use tildes to indicate the corresponding quantities in the lower 2×2 diagonal block of the matrix appearing in Eq. (93). Using Eqs. (97) and (98) in the definition of the Kraus operators, Eq. (76), we obtain:

$$\begin{aligned} K_0(t) &\equiv \sqrt{D_0(t)} \exp\left(i\frac{\varphi}{2}\right) (u_+^* \mathbb{I} + u_-^* \sigma_x) \\ &= \sqrt{D_0(t)} [|u_+| \mathbb{I} + \exp(i\varphi) |u_-| \sigma_x], \end{aligned} \quad (103)$$

$$\begin{aligned} K_1(t) &\equiv \sqrt{D_1(t)} \exp\left(i\frac{\varphi}{2}\right) (u_- \mathbb{I} - u_+ \sigma_x) \\ &= \sqrt{D_1(t)} [|u_-| \mathbb{I} - \exp(i\varphi) |u_+| \sigma_x], \end{aligned} \quad (104)$$

$$\begin{aligned} K_2(t) &\equiv \sqrt{D_2(t)} \exp\left(-i\frac{\tilde{\varphi}}{2}\right) (\tilde{u}_+^* \sigma_y + \tilde{u}_-^* \sigma_z) \\ &= \sigma_z \sqrt{D_2(t)} [|\tilde{u}_-| \mathbb{I} - i \exp(-i\tilde{\varphi}) |\tilde{u}_+| \sigma_x], \end{aligned} \quad (105)$$

and

$$\begin{aligned} K_3(t) &\equiv -\sqrt{D_3(t)} \exp\left(-i\frac{\tilde{\varphi}}{2}\right) (\tilde{u}_- \sigma_y - \tilde{u}_+ \sigma_z) \\ &= \sigma_z \sqrt{D_3(t)} [|\tilde{u}_+| \mathbb{I} + i \exp(-i\tilde{\varphi}) |\tilde{u}_-| \sigma_x]. \end{aligned} \quad (106)$$

Notice that, as we have already mentioned just following Eqs. (76) and (77), we have chosen phase factors whose convenience we clarify below.

Because $W(t)$, Eq. (97), is a unitary matrix, we have

$$|u_+|^2 + |u_-|^2 = 1 \quad (107)$$

and

$$|\tilde{u}_+|^2 + |\tilde{u}_-|^2 = 1, \quad (108)$$

so that each of the Kraus operators as defined in Eqs. (103-106) can be characterized by only three independent real numbers. Now let us apply each of these Kraus operators to the ket $|1\rangle$ of the qubit subspace we are considering, spanned by the basis set established in Eqs. (10) and (11), that is, $\{|1\rangle, |2\rangle\}$. Of course, this choice is arbitrary, but it is the analogous choice in the conventional Bloch-vector representation of qubit density operators [17]. Because of Eqs. (7) and (8), we obtain:

$$K_\gamma(t) |1\rangle = \sqrt{D_\gamma(t)} |\phi_\gamma\rangle, \quad (109)$$

for $\gamma = 0, 1, 2, 3$, where

$$|\phi_0\rangle = |u_+| |1\rangle + \exp(i\varphi) |u_-| |2\rangle, \quad (110)$$

$$|\phi_1\rangle = |u_-| |1\rangle - \exp(i\varphi) |u_+| |2\rangle, \quad (111)$$

$$|\phi_2\rangle = |\tilde{u}_-| |1\rangle + i \exp(-i\tilde{\varphi}) |\tilde{u}_+| |2\rangle, \quad (112)$$

and

$$|\phi_3\rangle = |\tilde{u}_+| |1\rangle - i \exp(-i\tilde{\varphi}) |\tilde{u}_-| |2\rangle. \quad (113)$$

Since Eqs. (107) and (108) hold, these four kets are normalized to unity and each one of them has a corresponding Bloch vector. Thus, for each ket of Eqs. (110-113) we define, respectively,

$$\begin{bmatrix} \cos\left(\frac{\theta_0}{2}\right) \\ \sin\left(\frac{\theta_0}{2}\right) \exp(i\varphi_0) \end{bmatrix} \equiv \begin{bmatrix} |u_+| \\ |u_-| \exp(i\varphi) \end{bmatrix}, \quad (114)$$

$$\begin{bmatrix} \cos\left(\frac{\theta_1}{2}\right) \\ \sin\left(\frac{\theta_1}{2}\right) \exp(i\varphi_1) \end{bmatrix} \equiv \begin{bmatrix} |u_-| \\ -|u_+| \exp(i\varphi) \end{bmatrix}, \quad (115)$$

$$\begin{bmatrix} \cos\left(\frac{\theta_2}{2}\right) \\ \sin\left(\frac{\theta_2}{2}\right) \exp(i\varphi_2) \end{bmatrix} \equiv \begin{bmatrix} |\tilde{u}_-| \\ i \exp(-i\tilde{\varphi}) |\tilde{u}_+| \end{bmatrix}, \quad (116)$$

and

$$\begin{bmatrix} \cos\left(\frac{\theta_3}{2}\right) \\ \sin\left(\frac{\theta_3}{2}\right) \exp(i\varphi_3) \end{bmatrix} \equiv \begin{bmatrix} |\tilde{u}_+| \\ -i \exp(-i\tilde{\varphi}) |\tilde{u}_-| \end{bmatrix}. \quad (117)$$

In view of the correspondence given by Eqs. (114-117), a convenient way to represent the Kraus operators of Eqs. (103-106) is, therefore, by four respective Bloch vectors in three dimensions, which we choose as the following:

$$\begin{aligned} \mathbf{v}_\gamma(t) &\equiv \sqrt{D_\gamma(t)} [\hat{\mathbf{x}} \sin \theta_\gamma \cos \varphi_\gamma \\ &\quad + \hat{\mathbf{y}} \sin \theta_\gamma \sin \varphi_\gamma + \hat{\mathbf{z}} \cos \theta_\gamma], \end{aligned} \quad (118)$$

for $\gamma = 0, 1, 2, 3$. Because of Eqs. (107) and (108), it follows that

$$|\mathbf{v}_\gamma(t)| = \sqrt{D_\gamma(t)},$$

for $\gamma = 0, 1, 2, 3$. Furthermore, we can derive from Eqs. (29) and (75) that

$$\sum_{\gamma=0}^3 D_\gamma(t) = 1.$$

As illustrations of the Kraus operators as three-dimensional vectors, Fig. 6 shows the complete trajectories of the vector representations of Eq. (118) for our four Kraus operators in the case in which we use $\rho_S(0) = |1\rangle\langle 1|$, $\omega_c = 8\pi/\tau$, $T = \hbar\omega_c/k_B$, $\eta = 0.05$, and $\Omega(t)$ as given by Eq. (55), with $n = 2$.

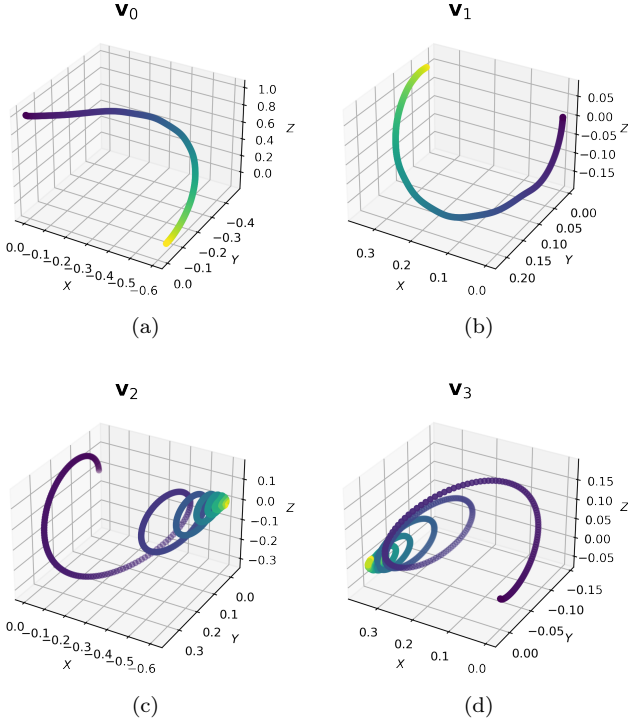


Figure 6: The complete trajectories of the vector representations of Eq. (118) for our four Kraus operators. Here we use $\rho_S(0) = |1\rangle\langle 1|$, $\omega_c = 8\pi/\tau$, $T = \hbar\omega_c/k_B$, $\eta = 0.05$, and $\Omega(t)$ as given by Eq. (55), with $n = 2$. Time evolution proceeds from purple (darker) to yellow (lighter).

The representation prescribed here shows the whole dynamics of the $\sqrt{\text{SWAP}}$ gate under the effects of dephasing mitigated by the procedure of dynamical decoupling. We advance this visualization recipe in the present context because the context, per se, is relevant. However, we also point out that we could apply the principles involved here for other qubit dynamics, although a graphical representation might usually be unpractical for qudit systems, as their state representation in terms of generalized Bloch vectors already indicates [32].

V. QUANTUM PROCESS TOMOGRAPHY IN THE LANGUAGE OF THE QUANTUM OPERATIONAL-PROBABILISTIC THEORY

Here we make the connection of the formalism just presented with the quantum OPT framework, which we briefly review in Appendix A. To reconstruct the Kraus operators (in other words, the dynamics) from measurement frequencies alone, we can measure the process matrix defined in Eq. (30) by means of QPT [33]. We wish to illustrate this technique using a simple OPT, with Positive Operator-Valued Measure (POVM) measurements [17]. This subject has been heavily discussed in the literature, and we point to Refs. [43–45] for a broad analysis of QPT, as well as Refs. [46, 47] for Quantum State Tomography (QST).

We describe the evolution of given preparations $\rho_i(0)$ by a generic noisy gate \mathcal{M} that acts on a qubit, of which we suppose having no knowledge. The index on the preparation tells us which initial condition we choose among Bloch vectors in the following set: $\{\mathbf{0}, \hat{x}, \hat{y}, \hat{z}\}$.

As in usual QST, we need a set of measurement operators to apply on the qubit. We choose the usual set

$$E_0 = |0_x\rangle\langle 0_x|, E_1 = |1_x\rangle\langle 1_x|, \quad (119)$$

$$E_2 = |0_y\rangle\langle 0_y|, E_3 = |1_y\rangle\langle 1_y|, \quad (120)$$

$$E_4 = |0_z\rangle\langle 0_z|, \text{ and } E_5 = |1_z\rangle\langle 1_z|. \quad (121)$$

A given element of this set is E_k . Notice that $E_{2j} + E_{2j+1}$ are all equal to the identity, for $j = 0, 1, 2$.

We describe the quantum process using its Kraus representation,

$$\mathcal{M}(\cdot) = \sum_{\alpha=0}^3 K_\alpha(\cdot)K_\alpha^\dagger, \quad (122)$$

with the condition

$$\sum_{\alpha=0}^3 K_\alpha^\dagger K_\alpha = \mathbb{I}. \quad (123)$$

Each probability is associated with a circuit as shown in Fig. 9 of Appendix A, with the detail that, as we do not control our process, $\mathcal{M}_j = \mathcal{M}, \forall j$. This probability can be written as

$$\begin{aligned} p_{i,k} &= \text{Tr}[\mathcal{M}(\rho_i(0))E_k] \\ &= \sum_{\alpha=0}^3 \text{Tr}[K_\alpha \rho_i(0) K_\alpha^\dagger E_k]. \end{aligned} \quad (124)$$

We represent each Kraus operator as a linear combination of the same σ_μ used in Eq. (28):

$$K_\alpha = \sum_{\mu=0}^3 k_\mu^\alpha \sigma_\mu. \quad (125)$$

Thus, we can write

$$\begin{aligned} p_{i,k} &= \sum_{\alpha=0}^3 \sum_{\mu=0}^3 \sum_{\nu=0}^3 \text{Tr}[k_{\mu}^{\alpha} k_{\nu}^{\alpha*} \sigma_{\mu} \rho_i(0) \sigma_{\nu} E_k] \\ &= \sum_{\mu=0}^3 \sum_{\nu=0}^3 M_{\mu\nu} \text{Tr}[\sigma_{\mu} \rho_i(0) \sigma_{\nu} E_k] \end{aligned} \quad (126)$$

where, by inspection, we notice that

$$M_{\mu\nu} = \sum_{\alpha=0}^3 k_{\mu}^{\alpha} k_{\nu}^{\alpha*} \quad (127)$$

is the same matrix defined in Eq. (30). An auxiliary definition is

$$Q_{\mu\nu}^{ik} := \text{Tr}[\sigma_{\mu} \rho_i(0) \sigma_{\nu} E_k], \quad (128)$$

which does not depend on the measurement frequencies themselves, but on the choice of measurement operators. The index k runs from zero to five, as we have six measurement operators, and the index i runs from zero to three, representing the four possible initial conditions of the Bloch vector. With these definitions, we obtain

$$\begin{aligned} p_{i,k} &= \sum_{\mu=0}^3 \sum_{\nu=0}^3 M_{\mu\nu} Q_{\mu\nu}^{ik} \\ &= \text{Tr}[M^T Q^{ik}]. \end{aligned} \quad (129)$$

If we define $|M\rangle$ as a column vector by stacking columns of M , and $|Q^{ikT}\rangle$ by stacking columns of $(Q^{ik})^T$, then

$$p_{i,k} = \langle Q^{ikT} | M \rangle.$$

Notice that we can define a 24-row vector $|p\rangle$ as

$$|p\rangle = \sum_{k=0}^5 \sum_{i=0}^3 p_{i,k} |4k+i\rangle, \quad (130)$$

where $4k+i$ indexes the vector row. In the same fashion, we define a 24×16 superoperator \mathcal{A} as

$$\mathcal{A} \equiv \sum_{k=0}^5 \sum_{i=0}^3 |4k+i\rangle \langle Q^{ikT}|. \quad (131)$$

These definitions lead us to

$$\mathcal{A} |M\rangle = |p\rangle, \quad (132)$$

from which it follows that

$$|M\rangle = (\mathcal{A}^T \mathcal{A})^{-1} \mathcal{A}^T |p\rangle. \quad (133)$$

As a self-consistency check, a comparison between M obtained by solving Eq. (31) or (32) numerically, then solving Eq. (58), and the one obtained by using the measurement frequencies given by Eq. (133) can be seen in Fig. 7. Figures 7(a) and 7(b) are diagrams of $\text{Re}[M]$ and $\text{Im}[M]$, respectively, obtained by Eq. (58). This M gives us probabilities via Eq. (124). These probabilities have

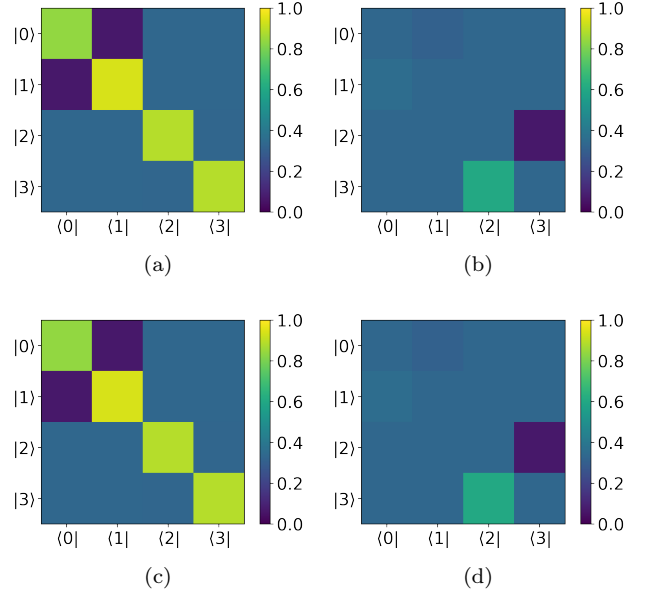


Figure 7: Figures (a) and (b): diagrams $\text{Re}[M]$ and $\text{Im}[M]$, obtained by solving Eq. (32). Figures (c) and (d): diagrams of the real and imaginary parts of tomographed M . In all figures, $t = \tau$, $\omega_c = 8\pi/\tau$, $T = \hbar\omega_c/k_B$, $\eta = 0.05$ and $\Omega(t)$ as given by Eq. (55) with $n = 2$.

been used in the method discussed above to reobtain M through Eq. (133). Figures 7(c) and 7(d) are diagrams of real and imaginary parts of this tomographed M , Eq. (133). In the calculations presented in Fig. 7 we used $t = \tau$, $\omega_c = 8\pi/\tau$, $T = \hbar\omega_c/k_B$, $\eta = 0.05$ and $\Omega(t)$ as given by Eq. (55) with $n = 2$.

As the matrices obtained by the procedures associated with Eqs. (58) and (133) are the same, we can de facto visualize the dynamics of a system by knowing only the frequencies of each measurement, given each initial state, since we can convert the process matrix M obtained by QPT, via Eq. (133), to a Kraus representation as explained in Sec. IV.

VI. CONCLUSION

In summary, we have considered the entangling universal quantum gate $\sqrt{\text{SWAP}}$ under the perturbation of a dephasing bath using a spin-boson Hamiltonian. Under the guidance of quantum operational-probabilistic theories, we argue for the importance of the calculation of Kraus operators, required to implement the completely-positive maps that are essential in the context of these theories. Usually one expects us to provide some means to overcome most of the deleterious effects of the decoherence promoted by the environmental noise. We accordingly have chosen continuous dynamical decoupling as such a protective control procedure and have calcu-

lated a set of Kraus operators for the residual dephasing. Inspired by the Bloch-vector trajectories which describe the reduced-state evolution of the system, in this case starting from an initial condition, we have prescribed a three-dimensional vector representation for the whole residual-noise dynamics, proving that such curves are sufficient to represent their corresponding Kraus-operator histories. We once again emphasize the relevance of the fact that the four Kraus-vector trajectories represent the whole dynamics of the qubit system, independently of its initial state. Finally, we have discussed the procedure to obtain the process matrix and, thus, the Kraus operators and their visual representation, in the OPT framework, where only a set of POVM measurement frequencies are assumed known.

Appendix A: Operational-Probabilistic Theories

References [28, 29] present the main ideas behind an OPT, with changes proposed by Ref. [30] to turn such a theory symmetric under time reversal. Reference [48], specially Chapter 4, explains how we can apply such a theory to a Stern-Gerlach weak-value problem.

An OPT is a theory that describes possible experiments to be done with physical apparatuses and gives predictions for outcomes of said experiments. It employs two basic notions: *systems* and *operations*. An operation represents a use of a physical device that connects systems to systems. Examples include a set of mirrors in an optical experiment or magnets in a Stern-Gerlach apparatus. Systems, as now may be clear, are the particles subject to the experimentation, as the atoms leaving the oven in a Stern-Gerlach setup.

Mathematically, systems are described by the usual Hilbert spaces. Operations are maps from systems to systems. As they are physical maps, they must be completely positive (CP) and trace preserving (TP). If a map is both CP and TP it is called a completely-positive and trace-preserving (CPTP) map.

An OPT has the advantage that it may be understood through diagrams as shown in Fig. 8. In Fig. 8(b) the box labeled by \mathcal{M} is an operation, where the index i represents an element of the set of outcomes. In this case, the wires A and B are systems. Systems evolve from left to right (e.g., we operate over the input system A with an operation \mathcal{M} and arrive at the output system B).

We may not care about our system before a given operation (in which case we hereon call such system “identity”). In terms of cooking, we usually do not care about, say, potatoes proceeding before cooking; we just wash and cook them (see Ref. [49] for the culinary example). This is called a *preparation*: we prepare the system so it is suitable to be studied in an experimental setting. In the diagram representation, we draw it with a curved input, as shown in Fig. 8(a). We may also not care about the system after a given operation (e.g., after eating a

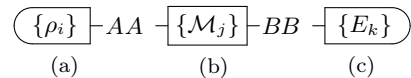


Figure 8: (a) is a preparation ρ , with possible outcomes indexed by i ; (b) is an operation \mathcal{M} , with possible outcomes indexed by j ; and (c) is a measurement E , with possible outcomes indexed by k .



Figure 9: Circuits represent probabilities.

meal); this is called *measurement* and we represent it with a curved output, as shown in Fig. 8(c).

We can compose preparations, operations and measurements in a closed (no open wires), non-cyclic (output from later operations cannot be used as input for previous operations) fashion, called *circuit* as done in Fig. 9. In an OPT, each circuit is associated with a probability. In other words, if we have a set of preparations $\{\rho_i\}_{i \in \mathcal{O}}$, operations $\{\mathcal{M}_j\}_{j \in \mathcal{Q}}$, and measurements $\{E_k\}_{k \in \mathcal{R}}$, then

$$p(i, j, k | \{\rho_i\}_{i \in \mathcal{O}}, \{\mathcal{M}_j\}_{j \in \mathcal{Q}}, \{E_k\}_{k \in \mathcal{R}}) \geq 0; \quad (\text{A1})$$

$$\sum_{i \in \mathcal{O}} \sum_{j \in \mathcal{Q}} \sum_{k \in \mathcal{R}} p(i, j, k | \{\rho_i\}_{i \in \mathcal{O}}, \{\mathcal{M}_j\}_{j \in \mathcal{Q}}, \{E_k\}_{k \in \mathcal{R}}) = 1 \quad (\text{A2})$$

For example, take a qubit in state $|0\rangle$ (which is our preparation) and operate a Hadamard gate H on it. Then, measure the probability of the qubit being at $|0\rangle$ or $|1\rangle$. Our preparation is, then, $\rho = |0\rangle\langle 0|$. Our operation is $\mathcal{M}(\cdot) = H(\cdot)H$. Our measurement can be either $E_1 = |0\rangle\langle 0|$ or $E_2 = |1\rangle\langle 1|$. Consider the usual probability rule. Then, the probability p_1 of measuring E_1 is

$$\begin{aligned} p_1 &= \langle \rho | \mathcal{M} | E_1 \rangle \\ &= \text{Tr}[\mathcal{M}(\rho)E_1] \\ &= \text{Tr}[H |0\rangle\langle 0| H |0\rangle\langle 0|] \\ &= \frac{1}{2} \text{Tr}[(|0\rangle\langle 0| + |1\rangle\langle 1|) |0\rangle\langle 0|] \\ &= \frac{1}{2}. \end{aligned} \quad (\text{A3})$$

In the same fashion, the probability p_2 of measuring

E_2 is

$$\begin{aligned}
p_2 &= \text{Tr}[\rho \mathcal{M} E_2] \\
&= \text{Tr}[H |0\rangle\langle 0| H |1\rangle\langle 1|] \\
&= \frac{1}{2} \text{Tr}[(|0\rangle\langle 0| + |1\rangle\langle 1|) |1\rangle\langle 1|] \\
&= \frac{1}{2}
\end{aligned} \tag{A4}$$

$$p_1 + p_2 = 1. \tag{A5}$$

These probabilities define an OPT. We make use of equivalence classes of operations: if we have two operations, $\{\mathcal{M}_j\}_{j \in \mathcal{Q}}$ and $\{\mathcal{N}_j\}_{j \in \mathcal{Q}}$, both with the same probability distributions for all preparations and measurements described in the theory, then they are considered the same operation. The same is valid both for preparations and measurements.

The probability associated with each circuit is a variation of the usual Hilbert-Schmidt inner product:

$$\begin{aligned}
p(i, j, k | \{\rho_i\}_{i \in \mathcal{O}}, \{\mathcal{M}_j\}_{j \in \mathcal{Q}}, \{E_k\}_{k \in \mathcal{R}}) \\
= \frac{\text{Tr}[\mathcal{M}_j(\rho_i) E_k]}{\sum_{i, j, k} \text{Tr}[\mathcal{M}_j(\rho_i) E_k]}
\end{aligned} \tag{A6}$$

where we associate the operations, usually maps, to matrices via isomorphism. If by happenstance there is an incompatibility of systems between operations (say, the output of \mathcal{M} is not compatible with the input of E for every possible outcome of \mathcal{M} and E), said probability is zero.

Such change on probability is needed because, as Ref. [30] points out, we need to define the constraints for measurements, as they do not necessarily follow POVM's constraints. Generally speaking, a measurement is a set of operators $\{E_k^A\}_{k \in \mathcal{R}}$ on system A , each event named *effect*, that follows

$$E_k^A \leq \sum_{k \in \mathcal{R}} E_k^A, \tag{A7}$$

$$\sum_{k \in \mathcal{R}} \text{Tr}[E_k^A] = d^A = \text{Tr}[\mathbb{I}^A]. \tag{A8}$$

An attentive reader notices that $\{E_k^B\}_{k \in \mathcal{R}}$ may be a POVM, but does not need to.

A preparation, set of operators $\{\rho_i^A\}_{i \in \mathcal{O}}$ in which each operator is called *state*, follows the density-matrix constraint:

$$\rho_i^A \leq \sum_{i \in \mathcal{O}} \rho_i^A, \tag{A9}$$

$$\sum_{i \in \mathcal{O}} \text{Tr}[\rho_i^A] = 1. \tag{A10}$$

Operations, set of CP maps $\{\mathcal{M}_j^{A \rightarrow B}\}_{j \in \mathcal{Q}}$ such that

each map is called a *transformation*, have the constraint

$$\mathcal{M}_j^{A \rightarrow B} \leq \sum_{j \in \mathcal{Q}} \mathcal{M}_j^{A \rightarrow B}, \tag{A11}$$

$$\sum_{j \in \mathcal{Q}} \text{Tr} \left[\mathcal{M}_j^{A \rightarrow B} \left(\frac{\mathbb{I}^A}{d^A} \right) \right] = 1. \tag{A12}$$

Appendix B: Derivation of $\xi(t)$

Here we briefly outline how to get the result of Eqs. (47) and (48). Using the evolution operator $U_I(t)$ in the interaction picture from Ref. [24] adapted to a single qubit, we can easily see that

$$\text{Tr}_B \left[U_I(t) |1\rangle \rho_B(0) \langle 1| U_I^\dagger(t) \right] = |1\rangle \langle 1| \tag{B1}$$

and

$$\text{Tr}_B \left[U_I(t) |2\rangle \rho_B(0) \langle 2| U_I^\dagger(t) \right] = |2\rangle \langle 2|, \tag{B2}$$

where $\rho_B(0)$ is given by Eq. (17). In the present context, of course, we are assuming $\Omega(t) = 0$ in Eqs. (21), (23), and (24). A somewhat more involved calculation gives

$$\begin{aligned}
\text{Tr}_B \left[U_I(t) |1\rangle \rho_B(0) \langle 2| U_I^\dagger(t) \right] &= |1\rangle \langle 2| \exp[\mathcal{P}(t)] \\
&\quad \times \exp[\mathcal{Q}(t)],
\end{aligned} \tag{B3}$$

where

$$\mathcal{P}(t) \equiv 4 \sum_s |g_s|^2 \frac{\cos(\omega_s t) - 1}{\omega_s^2}, \tag{B4}$$

$$\mathcal{Q}(t) \equiv 8 \sum_s \langle n_s \rangle |g_s|^2 \frac{\cos(\omega_s t) - 1}{\omega_s^2}, \tag{B5}$$

and we have used the very useful representation [39]:

$$\begin{aligned}
\rho_B(0) &= \prod_s \frac{1}{\langle n_s \rangle \pi} \\
&\quad \times \int d^2 \alpha_s \exp\left(-\frac{|\alpha_s|^2}{\langle n_s \rangle}\right) |\alpha_s\rangle \langle \alpha_s|,
\end{aligned} \tag{B6}$$

with

$$\langle n_s \rangle \equiv \frac{1}{\exp(\beta \hbar \omega_s) - 1} \tag{B7}$$

and $|\alpha_s\rangle$ is the usual coherent state for the s th mode of the boson bath. We can now use the spectral density given in the continuum description of Eqs. (41) and (42) to write Eq. (B4) as

$$\mathcal{P}(t) = 4\eta \int_0^\infty d\omega \exp\left(-\frac{\omega}{\omega_c}\right) \frac{\cos(\omega t) - 1}{\omega}. \tag{B8}$$

But,

$$\frac{\cos(\omega t) - 1}{\omega} = - \int_0^t dt' \sin(\omega t'), \tag{B9}$$

so that now Eq. (B8) gives

$$\mathcal{P}(t) = -2\eta \ln(1 + \omega_c^2 t^2). \quad (\text{B10})$$

Equation (B5) after using the spectral density given in the continuum description of Eqs. (41) and (42) and some algebraic manipulation can be put in this more convenient form:

$$\mathcal{Q}(t) = -8\eta \int_0^\infty d\omega \frac{\exp\left(-\frac{\omega}{\omega_c}\right)}{\exp(\beta\hbar\omega) - 1} \frac{1 - \cos(\omega t)}{\omega}, \quad (\text{B11})$$

It is an invigorating exercise to review some techniques of mathematical physics [40] to reexpress Eq. (B11) in the form

$$\mathcal{Q}(t) = \ln \left[\frac{\left| \left(\frac{k_B T}{\hbar\omega_c} + i \frac{k_B T}{\hbar} t \right)! \right|}{\left(\frac{k_B T}{\hbar\omega_c} \right)!} \right]^{8\eta}. \quad (\text{B12})$$

From the initial qubit density operator, $\rho_S(0) = |\psi_0\rangle\langle\psi_0|$, Eqs. (23), (45), (B1), (B2), (B3) with its Hermitian conjugate, and substitution of the results of Eqs.

(B10) and (B12), we finally obtain

$$\begin{aligned} \text{Tr}_B[\rho_I(t)] &= |c_1|^2 |1\rangle\langle 1| \\ &\quad + c_1 c_2^* \xi(t) |1\rangle\langle 2| \\ &\quad + c_1^* c_2 \xi(t) |2\rangle\langle 1| \\ &\quad + |c_2|^2 |2\rangle\langle 2|, \end{aligned} \quad (\text{B13})$$

where we have already recognized the definition of Eq. (48). Thus we see that Eq. (B13) is equivalent to Eq. (47).

ACKNOWLEDGMENTS

R.d.J.N. acknowledges support from Fundação de Amparo à Pesquisa do Estado de São Paulo (FAPESP), project number 2018/00796-3, and also from the National Institute of Science and Technology for Quantum Information (CNPq INCT-IQ 465469/2014-0) and the National Council for Scientific and Technological Development (CNPq). N. A. da C. M. acknowledges financial support from Coordenação de Aperfeiçoamento de Pessoal de Nível Superior (CAPES), project number 88887.339588/2019-00.

-
- [1] N. Khaneja, T. Reiss, C. Kehlet, T. Schulte-Herbrüggen, and S. J. Glaser, *Journal of Magnetic Resonance* **172**, 296 (2005).
- [2] S. Ashhab, P. C. de Groot, and F. Nori, *Phys. Rev. A* **85**, 052327 (2012).
- [3] T. J. Green, J. Sastrawan, H. Uys, and M. J. Biercuk, *New Journal of Physics* **15**, 095004 (2013).
- [4] J.-J. Zhu, X. Chen, H.-R. Jauslin, and S. Guérin, *Phys. Rev. A* **102**, 052203 (2020).
- [5] H. J. Kimble, *Nature* **453**, 1023 (2008).
- [6] S. Ritter, C. Nölleke, C. Hahn, A. Reiserer, A. Neuzner, M. Uphoff, M. Mücke, E. Figueroa, J. Bochmann, and G. Rempe, *Nature* **484**, 195 (2012).
- [7] M. Razavi, *An Introduction to Quantum Communications Networks*, 2053-2571 (Morgan & Claypool Publishers, 2018).
- [8] Y.-A. Chen, Q. Zhang, T.-Y. Chen, W.-Q. Cai, S.-K. Liao, J. Zhang, K. Chen, J. Yin, J.-G. Ren, Z. Chen, S.-L. Han, Q. Yu, K. Liang, F. Zhou, X. Yuan, M.-S. Zhao, T.-Y. Wang, X. Jiang, L. Zhang, W.-Y. Liu, Y. Li, Q. Shen, Y. Cao, C.-Y. Lu, R. Shu, J.-Y. Wang, L. Li, N.-L. Liu, F. Xu, X.-B. Wang, C.-Z. Peng, and J.-W. Pan, *Nature* **589**, 214 (2021).
- [9] M. Mirhosseini, A. Sipahigil, M. Kalaei, and O. Painter, *Nature* **588**, 599 (2020).
- [10] J. C. Budich and B. Trauzettel, *Nanotechnology* **21**, 274001 (2010).
- [11] S. B. Giddings and M. Rota, *Phys. Rev. A* **98**, 062329 (2018).
- [12] L. Bianchi, E. Compagno, V. Korepin, and S. Bose, *Quantum* **1**, 36 (2017).
- [13] M. Wang, Y. Xiang, H. Kang, D. Han, Y. Liu, Q. He, Q. Gong, X. Su, and K. Peng, *Phys. Rev. Lett.* **125**, 260506 (2020).
- [14] H.-Y. Liu, X.-H. Tian, C. Gu, P. Fan, X. Ni, R. Yang, J.-N. Zhang, M. Hu, J. Guo, X. Cao, X. Hu, G. Zhao, Y.-Q. Lu, Y.-X. Gong, Z. Xie, and S.-N. Zhu, *Phys. Rev. Lett.* **126**, 020503 (2021).
- [15] S. I. Bogdanov, A. Boltasseva, and V. M. Shalaev, *Science* **364**, 532 (2019).
- [16] B. M. Terhal, *Rev. Mod. Phys.* **87**, 307 (2015).
- [17] M. A. Nielsen, *Quantum Computation and Quantum Information: 10th Anniversary Edition* (Cambridge University Press, 2011).
- [18] A. Erhard, H. Poulsen Nautrup, M. Meth, L. Postler, R. Stricker, M. Stadler, V. Negnevitsky, M. Ringbauer, P. Schindler, H. J. Briegel, R. Blatt, N. Friis, and T. Monz, *Nature* **589**, 220 (2021).
- [19] S. L. Bayliss, D. W. Laorenza, P. J. Mintun, B. D. Kivos, D. E. Freedman, and D. D. Awschalom, *Science* **370**, 1309 (2020).
- [20] F. Nosrati, A. Castellini, G. Compagno, and R. Lo Franco, *npj Quantum Information* **6**, 39 (2020).
- [21] J. H. Becher, E. Sindici, R. Klemm, S. Jochim, A. J. Daley, and P. M. Preiss, *Phys. Rev. Lett.* **125**, 180402 (2020).
- [22] D. Lacroix, *Phys. Rev. Lett.* **125**, 230502 (2020).
- [23] M. Anderlini, P. J. Lee, B. L. Brown, J. Sebby-Strabley, W. D. Phillips, and J. V. Porto, *Nature* **448**, 452 (2007).
- [24] J. H. Reina, L. Quiroga, and N. F. Johnson, *Phys. Rev. A* **65**, 032326 (2002).
- [25] F. F. Fanchini, J. E. M. Hornos, and R. d. J. Napolitano, *Phys. Rev. A* **75**, 022329 (2007).
- [26] K. Kraus, *States, Effects, and Operations: Fundamental Notions of Quantum Theory (Lecture Notes in Physics)* (Springer, 1983).
- [27] M. Keyl, *Physics Reports* **369**, 431 (2002).

- [28] G. Chiribella, G. M. D'Ariano, and P. Perinotti, *Phys. Rev. A* **81**, 062348 (2010).
- [29] G. Chiribella, G. M. D'Ariano, and P. Perinotti, *Phys. Rev. A* **84**, 012311 (2011).
- [30] O. Oreshkov and N. J. Cerf, *Nature Physics* **11**, 853 (2015).
- [31] P. Kurzyński, A. Kołodziejcki, W. Laskowski, and M. Markiewicz, *Phys. Rev. A* **93**, 062126 (2016).
- [32] R. A. Bertlmann and P. Krammer, *Journal of Physics A: Mathematical and Theoretical* **41**, 235303 (2008).
- [33] I. L. Chuang and M. A. Nielsen, *Journal of Modern Optics* **44**, 2455 (1997).
- [34] A. O. Caldeira and A. J. Leggett, *Phys. Rev. Lett.* **46**, 211 (1981).
- [35] A. J. Leggett, S. Chakravarty, A. T. Dorsey, M. P. A. Fisher, A. Garg, and W. Zwerger, *Rev. Mod. Phys.* **59**, 1 (1987).
- [36] F. Shibata, Y. Takahashi, and N. Hashitsume, *Journal of Statistical Physics* **17**, 171 (1977).
- [37] S. Chaturvedi and F. Shibata, *Zeitschrift für Physik B Condensed Matter* **35**, 297 (1979).
- [38] K. Blum, *Density Matrix Theory and Applications: 64 (Springer Series on Atomic, Optical, and Plasma Physics)* (Springer, 2012).
- [39] C. W. Gardiner and P. Zoller, *Quantum noise: a handbook of Markovian and non-Markovian quantum stochastic methods with applications to quantum optics* (Springer-Verlag, Berlin Heidelberg, 2004).
- [40] G. B. Arfken, *Mathematical Methods for Physicists: A Comprehensive Guide* (Academic Press, 2011).
- [41] A. Uhlmann, *Reports on Mathematical Physics* **9**, 273 (1976).
- [42] R. Jozsa, *Journal of Modern Optics* **41**, 2315 (1994).
- [43] M. Mohseni, A. T. Rezakhani, and D. A. Lidar, *Physical Review A* **77**, 032322 (2008).
- [44] G. Gutoski and N. Johnston, *Journal of Mathematical Physics* **55**, 032201 (2014), arXiv: 1309.0840.
- [45] G. Torlai, C. J. Wood, A. Acharya, G. Carleo, J. Carrasquilla, and L. Aolita, arXiv:2006.02424 [quant-ph] (2020), arXiv: 2006.02424.
- [46] J. B. Altepeter, D. F. V. James, and P. G. Kwiat, "Quantum state tomography," (2004).
- [47] M. A. Heno and M. Restrepo, "Reconstruction of single and 2-qubit density matrices using quantum state tomography," (2017).
- [48] N. A. d. C. Morazotti and R. d. J. Napolitano, *Reversão temporal na linguagem operacional da mecânica quântica e a evolução temporal de pacotes de onda para espalhamento*, Master's thesis, Universidade de São Paulo, Instituto de Física de São Carlos (2018).
- [49] B. Coecke, *Contemporary Physics* **51**, 59 (2010).